PERGAMON

International Journal of Heat and Mass Transfer 43 (2000) 2245–2256

International Journal of HEAT and MASS TRANSFER

www.elsevier.com/locate/ijhmt

Thermal management of high power electronics with phase change cooling

T.J. Lu

Department of Engineering, Cambridge University, Cambridge CB2 1PZ, UK

Received 24 June 1999; received in revised form 18 October 1999

Abstract

A study on the prospect of designing high power electronic packages with phase change cooling is presented, with special emphasis on minimising the rising of junction temperatures due to thermal transient effects. The one-dimensional thermal model consists of a finite slab suddenly exposed to a uniform heat flux at the top surface and cooled by convective air at the bottom. The phase change problem is divided into sub-problems and solved progressively. Before the slab starts to melt, both exact and approximate solutions are presented for the distribution of temperature in the slab as functions of time and Biot number Bi. The necessity of partitioning the time domain into two regimes, separated by the time t_0 needed for the thermal front to traverse across the whole slab, is emphasised. After the slab melts, quasi-steady state solutions are obtained both for the melt depth and the evolution of surface temperature as functions of time and Biot number when $t_m > t_0$, with t_m denoting the time needed for melting to commence at the top surface of the slab. The quasi-steady state solutions are compared with those obtained by using the method of finite elements. Approximate but simple analytical solutions are also constructed for the $t_m < t_0$ case which, again, are compared with the finite element results. Finally, these solutions are analysed to guide the design of advanced packages with optimised phase change cooling strategies.

Keywords: Phase change cooling; Power electronics; Thermal management; Finite elements; Materials selection

1. Introduction

One of the key barriers for developing next-generation high power electronic packages with power densities in excess of 10^7 W/m^2 has been the minimisation of junction temperatures without liquid cooling [1–3]. The situation becomes even more conspicuous when the device experiences a sudden surge of power density due to, for instance, lightening. To meet the requirement on the safe operation area of the device, it has been proposed to reduce the thermal resistance of the device by phase change cooling, in addition to air convection. It is the aim of this study to analyse the feasibility of using such a cooling strategy on power electronic packages whose maximum safe operating temperature is around 400°C.

The generic problem to be analysed is schematically shown in Fig. 1, where the top surface of a thin layer of phase change material is suddenly exposed to a heat flux of intensity Q. The top surface of the layer is attached to the Si chip (the heat source, not shown in the figure) whereas its bottom surface is cooled by convective air. For a given heat flux intensity Q, the geometry and thermophysical properties of the phase change layer need to be optimised such that the temperature achieved at the top surface of the layer is kept below the maximum allowable temperature. In reality, the phase change material is separated from

E-mail address: TJL21@eng.cam.ac.uk (T.J. Lu).

0017-9310/00/$ - see front matter
PII: S0017-9310(99)00318-X

Nomenclature

Bi	Biot number
c_s, c_l	solid and melt specific heat
h	local heat transfer coefficient
H	phase change layer thickness
I_1, I_2	material indices
k_s, k_l	solid and melt thermal conductivities
L	latent heat
Q	heat flux
t	time
t_c	time for complete melting
t_0	thermal penetration time
t_m	melting time
T_0	initial and environmental temperature
T_m, T_v	melting and boiling temperatures
T_s, T_l	solid and melt temperatures
x	coordinate
X	melt front position

Greek symbols

ΔT	$\equiv T_m - T_0$
κ_s, κ_l	solid and melt thermal diffusivities
ρ	density

Subscripts

l	liquid
s	solid

direct air cooling by a substrate (e.g., AIN). The substrate must be thin and conduct heat well, in addition to other requirements such as thermal expansion matching and low dielectric constant, and hence the assumption of an effective coefficient of heat transfer equal to that of air convection at the substrate surface holds (see Appendix).

The problem as shown in Fig. 1 belongs to a class of heat transfer problems generally known as the 'Stefan problem' which finds prevalent applications in areas such as welding, laser material processing, optical recording, laser shock hardening, local diffusion and alloying, laser annealing of semiconductor thin films, energy storage, and freezing/thawing of soils and foodstuffs [4–9]. Despite of obvious widespread interests, the Stefan problems have no general solutions: even for a few special cases such as a semiinfinite solid with the prescribed

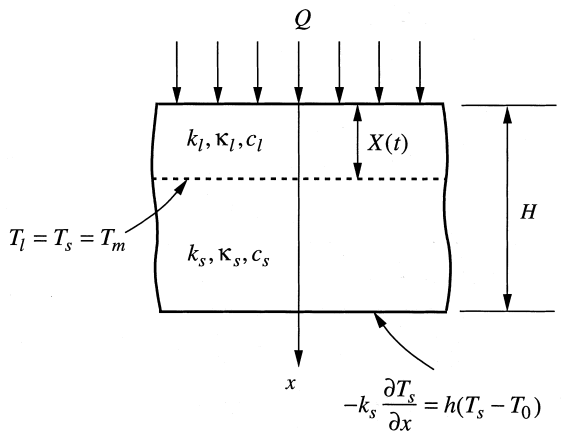

Fig. 1. Geometry and boundary conditions for transient heat transfer in a single layer.

temperature boundary conditions, assumptions must be made regarding the temperature profiles either in the solid or liquid. For the solidification of a semi-infinite liquid medium initially at melting temperature and subjected to a uniform heat flux at the surface, an approximate series solution is given in Ref. [10]. The same problem is solved later by Cohen [5] using the method of electrical analogy, and by Xie and Kar [8] with a semi-empirical approach. The solutions to the inverse Stefan problems, wherein the boundary conditions are specified at the moving rather than the fixed boundary, are discussed by Gibson [11] and Rubinsky and Shitzer [12]. Assuming that the liquid is maintained at its melting temperature, El-Adawi [7] develops an approximate analytical method for the problem as specified in Fig. 1. A numerical technique based on finite difference for solving multi-dimensional melting problems is presented by Lazaridis [13], whereas the method of heat balance integral is developed by Goodman [14] to obtain approximate solutions for the Stefan problems. The detection of laser-induced melt at the surface of a solid in real time is demonstrated using a photothermal deflection technique by Shannon et al. [15]. These authors also derived a quasi-steady state solution for the melting front in spherical coordinates due to a point source.

In the present paper, the complete mathematical model for the problem of Fig. 1 is described in Section 2 and solved progressively in Sections 3–5. The exact solution for the distribution of temperature in the phase change material before melting is presented in Section 3, followed by an approximate but much simpler solution obtained using the variational formulation. The evolution of temperature is conveniently divided into two regimes I and II, separated by the thermal penetration time t_0 needed for the heat front

to penetrate from the top surface of the layer to the bottom. The solution for regime I is identical to that of a semi-infinitely large medium exposed to a constant heat flux at the surface and thermally insulated at infinity. Section 4 presents approximate analytical solutions for the melt depth and the temperature of the top surface, each as a function of time, with the assumption that the applied heat flux has an intensity sufficiently low such that quasi-steady state temperature profiles hold inside the melted as well as the unmelted regimes. The range of validity of the quasi-steady state solutions is discussed relative to those obtained from the finite element method (FEM). In Section 5, the solutions for the melting depth and temperature distribution due to high heat flux intensities are obtained by using an approximate analytical technique as well as FEM. Finally, in Section 6, these solutions are used to optimise the design strategy of phase change cooling for advanced power packages with prescribed performance specifications.

2. Specifications of the problem

The top surface of an isotropic and homogeneous layer of initial temperature T_0 is suddenly exposed to a uniform heat flux Q at time $t = 0$ (Fig. 1). It is assumed that the layer has a thickness H small compared with its other dimensions such that the loss of heat from the sides is negligible, and that the surface area of the layer is sufficiently large to allow the heat being conducted perpendicularly to its top surface. As part of the heat may be dissipated away due to radiation and convection to the ambient, Q is treated here as the net heat flux absorbed by the layer and independent of time t. Before melting, a portion of the input heat is consumed on raising the temperature of the layer, the rest being lost to the environment of temperature T_0 via the bottom surface of the layer at $x = H$ where a constant convective heat transfer coefficient h is assumed. (Here, for simplicity, the initial temperature of the phase change layer is assumed to be equal to the temperature of the cooling medium; this assumption can be relaxed if necessary.) Let T_m be the melting temperature of the material of which the layer is made and L the corresponding latent heat. Then, after the top surface temperature reaches T_m, a portion of the heat is also lost due to phase change (melting). Let k_s, κ_s, c_s denote respectively the thermal conductivity, diffusivity and specific heat (at constant pressure) of the solid material, k_l, κ_l, c_l the corresponding properties of the liquid material after melting, and assume the liquid and solid have identical density ρ. Let $X(t)$ represent the line of melting front separating the liquid and solid phases. Under these conditions, a one-dimensional analysis of the problem is appropriate and the temperature of the layer may be expressed as $T_s \equiv T_s(x, t)$ for the solid and $T_l \equiv T_l(x, t)$ for the liquid.

For linear flow, the one-dimensional conduction of heat in the liquid and solid must satisfy

$$\frac{\partial^2 T_l}{\partial x^2} = \frac{1}{\kappa_l}\frac{\partial T_l}{\partial t}, \quad 0 \le x \le X(t) \tag{1a}$$

$$\frac{\partial^2 T_s}{\partial x^2} = \frac{1}{\kappa_s}\frac{\partial T_s}{\partial t}, \quad X(t) \le x \le H \tag{1b}$$

where constant thermophysical properties are assumed due to a dearth of data on the temperature dependence of these properties. The thermal conductivity of some common phase change materials may increase by 10–30% as the temperature is increased from 0 to 400°C [16]. This variation, if included, is not expected to significantly affect the phase change phenomena discussed in this work. The initial and boundary conditions appropriate for the problem are

$$T_l(x, 0) = T_s(x, 0) = T_0, \quad \text{at } t = 0 \tag{2}$$

$$-k_l\frac{\partial T_l}{\partial x} = Q, \quad \text{at } x = 0 \tag{3}$$

$$k_s\frac{\partial T_s}{\partial x} - k_l\frac{\partial T_l}{\partial x} = \rho L\frac{dX}{dt}, \quad \text{at } x = X(t) \tag{4}$$

$$T_l(x, t) = T_s(x, t) = T_m, \quad \text{at } x = X(t) \tag{5}$$

$$-k_s\frac{\partial T_s}{\partial x} = h\{T_s(H, t) - T_0\}, \quad \text{at } x = H \tag{6}$$

$$X(t) = 0, \quad t \le t_m \tag{7}$$

where t_m is the time needed for the top surface of the layer to melt. The problem of melting as specified by Eqs. (1)–(7) is nonlinear due to the fact that the velocity of the melting front is coupled to the temperature via Eq. (4). The solution presented below applies to a motionless solid/liquid medium where the change of volume due to melting is neglected (i.e., $\rho_l = \rho_s = \rho$).

It should be pointed out that, for applications such as high power electronic packages, the phase change material is usually placed on top of a substrate cooled by air convection, and hence the coefficient h introduced in Eq. (6) is taken as an effective heat transfer coefficient in the sense that it accounts for contributions from two sources: one from convection at the bottom of the substrate and the other from heat conduction across the substrate. However, as demon-

strated in Appendix, if the substrate is thin and conducts heat well (which is a valid assumption for modern power electronics packages), h would essentially be the same as the convective heat transfer coefficient at the bottom surface of the substrate.

3. Solutions before melting

In this section, exact and approximate solutions for the temperature distribution inside a heated layer before melting are presented and compared. These temperature profiles constitute the basis for the subsequent analysis of melting in Sections 4 and 5. In addition, the importance of partitioning the time domain into two regimes is emphasised.

3.1. Temperature profiles

In the absence of melting ($X(t) \equiv 0$), Eqs.(1)–(3), together with the convective heat transfer boundary condition (6), can be solved by the method of Laplace transform [10], yielding

$$\frac{T_s(x,t)-T_0}{Q} = \frac{H-x}{k_s} + \frac{H}{k_s}\left\{\frac{1}{Bi} - 2\sum_{n=1}^{\infty}\frac{e^{-\lambda_n^2 k_s t/H^2}\cos(\lambda_n x/H)}{\lambda_n(\lambda_n + \sin\lambda_n \cos\lambda_n)}\right\} \tag{8}$$

Here, the nondimensional heat transfer coefficient, Bi, is the Biot number defined as $Bi = hH/k_s$ and λ_n are the positive roots of the transcendental equation

$$\lambda_n \tan\lambda_n = Bi \tag{9}$$

In the limit $Bi \to \infty$ (i.e., constant temperature boundary condition at $x = H$), $\lambda_n = (2n+1)\pi/2$ reducing Eq. (8) to

$$\frac{T_s(x,t)-T_0}{Q} = \frac{2\sqrt{\kappa_s t}}{k}\sum_{n=1}^{\infty}(-1)^n\left\{\text{ierfc}\frac{2nH+x}{2\sqrt{\kappa_s t}} - \text{ierfc}\frac{2(n+1)H-x}{2\sqrt{\kappa_s t}}\right\}$$
$$= \frac{H-x}{k_s} - \frac{8H}{k_s\pi^2}\sum_{n=0}^{\infty}(-1)^n \times \frac{e^{-(2n+1)^2\pi^2\kappa_s t/4H^2}}{(2n+1)^2}\sin\frac{\pi(2n+1)(H-x)}{2H} \tag{10}$$

where the function 'ierfc' is defined in terms of the error function 'erf' as

$$\text{ierfc}\, x \equiv \frac{e^{-x^2}}{\sqrt{\pi}} - x(1-\text{erf}\, x) \tag{11}$$

If, on the other hand, the bottom surface of the layer is thermally insulated with $Bi = 0$ then $\lambda_n = n\pi$. For finite values of Bi, the coefficients λ_n are bounded by the above two limiting cases as

$$n\pi < \lambda_n < \frac{(2n+1)\pi}{2}, \quad n = 0, 1, 2, \ldots \tag{12}$$

but otherwise λ_n must be determined numerically.

Although the solution (8) to the temperature distribution is exact, it involves the evaluation of the sum of an infinite series, which is non-trivial. An approximate but much simpler solution to the problem can be obtained using the variation formulation, coupled with the Kantorovich method [17], resulting in

$$\frac{T_s(x,t)-T_0}{Q} = \frac{\sqrt{5\kappa_s t}}{2k_s}\left(1 - \frac{x}{\sqrt{5\kappa_s t}}\right)^2, \quad \text{when } 0 \le t \le t_0$$
$$= \frac{(H-x)^2}{2k_s H} + \frac{H}{k_s} \times \left(\frac{1}{Bi} + \frac{H^2-x^2}{2H^2}\right)\left\{1 - e^{-\frac{\kappa_s(t-t_0)(1+Bi/3)}{H^2(2/3+2Bi/15+1/Bi)}}\right\}, \quad \text{when } t \ge t_0 \tag{13}$$

where $t_0 = H^2/5\kappa_s$ is the penetration time of the applied heat flux to the bottom surface ($x = H$) of the layer and is independent of the amount of heat being conducted. (Notice that the exact solution (8) gives $t_0 = \pi H^2/16\kappa_s$, slightly smaller than that given by the approximate method $t_0 = H^2/5\kappa_s$). For semi-infinitely thick layers ($H \to \infty$), the solution simplifies to

$$\frac{T_s(x,t)-T_0}{Q} = \frac{2\sqrt{\kappa_s t}}{k_s}\text{ierfc}\frac{x}{2\sqrt{5\kappa_s t}}, \quad \text{exact}$$
$$= \frac{\sqrt{5\kappa_s t}}{2k_s}\left(1 - \frac{x}{\sqrt{5\kappa_s t}}\right)^2, \quad \text{approximate} \tag{14}$$

Selected numerical calculations indicate that, before melting takes place, Eq. (13) accurately describes the evolution of temperature in the layer, particularly so if the material is near either surface of the layer or if $t > t_0$, with an error typically less than 1%.

In the limit $t \to \infty$, both Eqs. (8) and (13) reduce to the steady-state result

$$\frac{T_{\text{steady state}} - T_0}{Q} = \frac{H}{k_s}\left(\frac{1}{Bi} + \frac{H-x}{H}\right) \tag{15}$$

It follows that the maximum temperature the top surface of the layer may reach is $T^{\max}_{\text{surface}} = T_0 + (QH/k_s) \times (1 + 1/Bi)$. However, since melting occurs as soon as $T_{\text{surface}} = T_m$ the actual surface temperature would be lower than that dictated by $T^{\max}_{\text{surface}}$, which is also bounded by the boiling temperature of the material T_v.

3.2. Temperature regimes I and II

As shown in Eq. (13), there exist two regimes for the temperature distribution in a layer of thickness H, namely, $t < t_0$ (regime I) and $t > t_0$ (regime II). In regime I, the bottom surface of the layer is yet to be affected by the penetration of heat flow such that $T_s(H, t) \equiv T_0$. As a result, the temperature distribution across the layer is identical to that for a semi-infinite medium satisfying $\lim_{x\to\infty} T_s(x, t) = T_0$, [5], with all of the heat consumed on raising the temperature of the material. In regime II, part of the heat is lost to the environment via the bottom surface $x = H$, causing the temperature distribution inside the layer to depend on both the layer thickness H and heat transfer coefficient h. Given that the characteristics of melting in regime I are, in general, different from those in Regime II, the two regimes should be dealt with separately.

At $t = t_0$, the temperature attained at the top surface of the layer is readily calculated from Eq. (13), as

$$\frac{T_{\text{surface}}(t_0)}{T_m} = \frac{T_0}{T_m} + \frac{QH}{2k_s T_m} \tag{16}$$

which depends linearly on the layer thickness H. Also, from Eq. (13), the time needed for the top surface of the layer to melt, t_m, is

$$\frac{t_m}{t_0} = \begin{cases} \left(\dfrac{2k_s\Delta T}{QH}\right)^2, & \text{if } t_m \le t_0 \\ 1 - \dfrac{2}{m}\ln\left\{1 - \left(\dfrac{2k_s\Delta T}{QH} - 1\right)\dfrac{Bi}{2+Bi}\right\}, & \text{if } t_m \ge t_0 \end{cases} \tag{17}$$

where $\Delta T = T_m - T_0$ and m is a dimensionless parameter given by

$$m = \frac{2\kappa_s t_0(1 + Bi/3)}{H^2(2/3 + 2Bi/15 + 1/Bi)} \tag{18}$$

With the assumption that $T_0 = 300$ K, Fig. 2 presents the reciprocal of t_m/t_0 as a function of layer thickness H for two heat flux intensities: $Q = 10^8$ and $Q = 10^9$ W/m^2, and for four materials: aluminium, copper, titanium and fused quartz. The thermophysical properties of these materials as given by Xie and Kar [8] are listed in Table 1. It is seen from Fig. 2(a) that for a layer of thickness 0.5 mm and heat flux $Q = 10^8$ W/m^2, among the four materials only fused quartz has started melting when $t = t_0$. On the other hand, if the heat flux is increased to $Q = 10^9$ W/m^2, other conditions unchanged, then all materials except copper have started to melt after an elapse of time t_0. Consequently, the analysis of melting in a finite slab should in general consist of two parts, one for melting time t_m less than t_0 and the other for t_m longer than t_0.

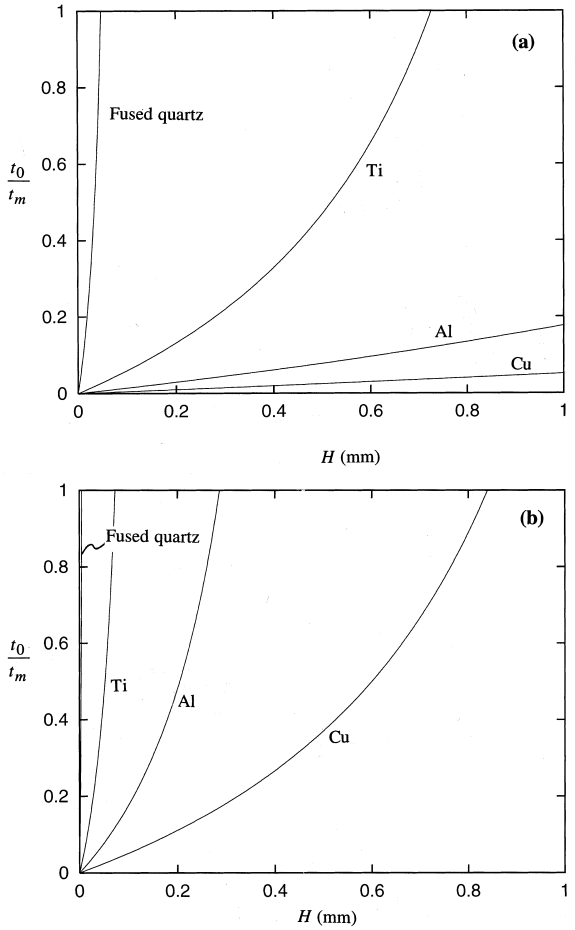

Fig. 2. Dimensionless time to melting t_m/t_0 as a function of layer thickness H for (a) $Q = 10^8$ W/m^2, (b) $Q = 10^9$ W/m^2, with $T_0 = 300$ K and $h = 5$ W/(m^2 K).

4. Solutions for low power densities ($t_m > t_0$)

4.1. Quasi-steady state solutions

The problem of melting with a moving boundary has no general solution [10,18]. Although approximate analytical solutions are available for a few simplified cases with phase changes occurring at constant temperature, numerical methods such as finite difference

and finite elements are commonly used to deal with more complicated problems.

If, however, the applied heat flux has an intensity typically less than 10^9 W/m^2 and the layer of phase change material is thin (<1 mm for power packaging applications), the concept of 'quasi-steady state' may be used to arrive at approximate analytical solutions both for the position of the melting line and the surface temperature of the layer as functions of time.

The method of quasi-steady state assumes that the variation of temperature with time is slow during melting such that the temperature gradients both in the molten layer and solid layer are approximately constant, although these may change with time. Under this assumption, the temperature profile in the liquid region at present time t may be taken as

$$T_l(x,t) = T_m - \frac{Q}{k_l}\{x - X(t)\}, \quad x \le X(t) \tag{19}$$

which satisfies both Eqs. (3) and (5). Similarly, in the solid region, the temperature distribution satisfying the boundary conditions (5) and (6) takes the form

$$T_s(x,t) = T_m - \frac{(T_m - T_0)\{x - X(t)\}}{H\{1 - X(t)/H + 1/Bi\}}, \quad X(t) \le x \le H \tag{20}$$

Substitution of the above temperature profiles into the enthalpy balance equation (4) leads to the following parameteristic equation for $X(t)$

$$\frac{X(t)}{H} - \frac{k_s \Delta T}{HQ}\ln\left\{1 - \frac{X(t)}{H}\left(1 + \frac{1}{Bi} - \frac{k_s \Delta T}{HQ}\right)^{-1}\right\} = \frac{Q(t - t_m)}{\rho L H} \tag{21}$$

where $\Delta T = T_m - T_0$. The solution obtained from Eq. (21) is approximate in the sense that the proposed temperature profiles (19) and (20) do not satisfy the energy equation (1); they do, however, preserve the energy balance at the melting front, i.e., Eq. (4).

Table 1
Thermophysical properties of selected materials

	Aluminium	Copper	Titanium	Fused quartz
k_s (W/(m K))	226	397	22	1.67
κ_s (10^{-6} m^2/s)	96.8	115	9.6	0.73
k_l (W/(m K))	92	170	28	2.87[a]
κ_l (10^{-6} m^2/s)	38	43	8.23	1.5[a]
ρ (kg/m^3)	2700	8960	4510	2650
T_m (K)	933	1358	1953	1743
T_v (K)[b]	2723	2833	3533	2270
L (10^5 J/kg)	3.97	2.05	4.37	1.46

[a] Data at 1500 K.
[b] Boiling temperature.

For thin layers coupled with air convection, $Bi = hH/k_s < 1$, thus Eq.(21) is reduced to

$$\frac{X(t)}{H} = \frac{Q(t - t_m)}{\rho L H(1 + h\Delta T/Q)} \tag{22}$$

Given that $h \sim 10$ W/(m^2 K) for air cooling, $Q \sim 10^6$–10^{10} W/m^2 for most applications, and $\Delta T \sim 100$–1000 K, $h\Delta T \ll Q < 1$, and hence the above solution for the location of the melting front can be further simplified to

$$X(t) = \frac{Q(t - t_m)}{\rho L} \tag{23}$$

which has a constant velocity $Q/\rho L$. From Eqs. (19) and (23), the temperature at the top surface of the phase change layer is obtained as

$$T_{surface}(t) = T_m + \frac{Q^2}{\rho k_l L}(t - t_m), \quad t \ge t_m \tag{24}$$

where, for $Bi \ll 1$,

$$\frac{t_m}{t_0} = 5\left(\frac{k_s T_m}{QH}\right)\left(1 - \frac{T_0}{T_m}\right) - 1.5 \tag{25}$$

Thus, when $Bi \ll 1$, the complete solution for the surface temperature as a function of time can be summarised from Eqs. (13) and (24) as follows

$$\frac{T_{surface}(t) - T_0}{Q} = \begin{cases} \dfrac{\sqrt{5\kappa_s t}}{2k_s}, & 0 \le t \le t_0 \\ \dfrac{H}{2k_s} + \dfrac{t - t_0}{\rho c_s H}, & t_0 \le t \le t_m \\ \dfrac{T_m - T_0}{Q} + \dfrac{Q}{\rho k_l L}(t - t_m), & t \ge t_m \end{cases} \tag{26}$$

After melting has occurred, the surface temperature as given by Eq. (26) can also be conveniently written in the following non-dimensional form

$$\frac{T_{surface}(t) - T_0}{T_m - T_0} = 1 + \frac{Ste}{5}\left(\frac{k_s}{k_l}\right)\left[\frac{QH}{k_s(T_m - T_0)}\right]^2 \times \left(\frac{t}{t_0} - \frac{t_m}{t_0}\right), \quad t \ge t_m \tag{27}$$

where $Ste = c_s(T_m - T_0)/L$ is the Stefan number, with $t_0 = H^2/5\kappa_s$. The Stefan number is a dimensionless measures of the degree of superheating that is being experienced by the liquid. For materials having rela-

tively high melting points, the value of *Ste* is of the order of unity.

Fig. 3(a) presents the predicted variation of melt depth with time, $X(t)$, in a layer of thickness $H = 1$ mm for two power densities: $Q = 10^7$ and $Q = 5 \times 10^6$ W/m^2. The corresponding evolution of surface temperature with time, $T_{surface}(t)$, is plotted in Fig. 3(b). The parameters used for the plotting are $T_0 = 300$ K, $T_m = 673$ K, $L = 10^5$ J/kg, $k_s = k_l = 100$ W/(m K), $\rho = 1000$ kg/m^3, $c_s = c_l = 500$ J/(kg K) and $h = 10$ W/(m^2 K). The same one-dimensional problem is also solved by using the finite element code ABAQUS; the results for $X(t)$ and $T_{surface}(t)$ are shown in Fig. 3 as the solid lines, which agree closely with those calculated from the quasi-steady state method (the dashed lines). (A brief description of the finite element method as used for melting problems will be given in the next section.) Fig. 3 suggests that although the quasi-steady state solutions somewhat overestimate the effect of power density on both $X(t)$ and $T_{surface}(t)$, the behavioural trends are correctly predicted: before melting, $X(t)$ and $T_{surface}(t)$ increase nearly linearly and quadratically, respectively; after melting, both $X(t)$ and $T_{surface}(t)$ increase linearly.

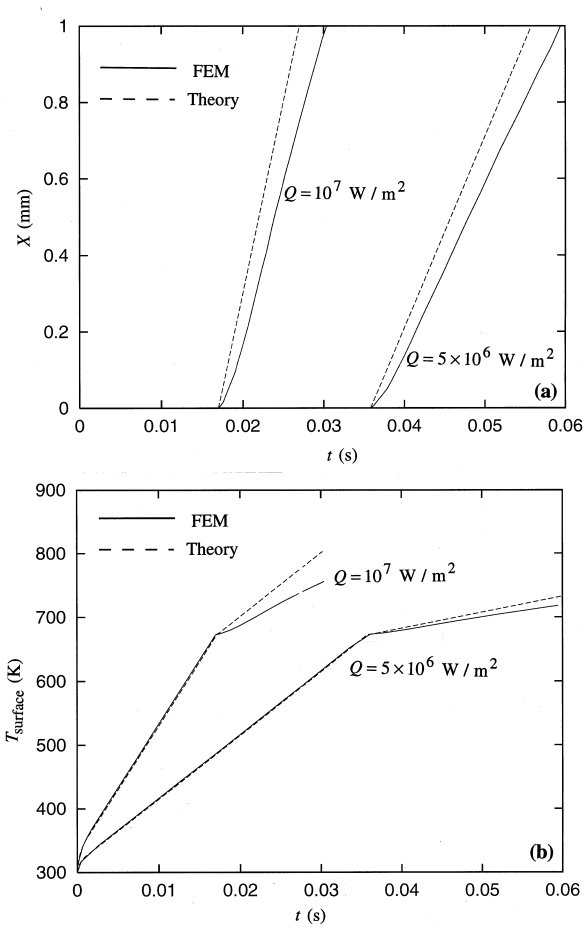

Fig. 3. (a) Melt depth $X(t)$, (b) surface temperature $T_{surface}(t)$ as functions of time for two heat flux intensities: $Q = 10^7$ and $Q = 5 \times 10^6$ W/m^2. Quasi-steady state solutions are represented as dashed lines and FEM results as solid lines. The other parameters used are $H = 1$ mm, $k_s = 100$ W/(m K), $L = 10^5$ J/kg, $\rho = 10^3$ kg/m^3, $c_s = 500$ J/(kg K), $h = 10$ W/(m^2 K), $T_0 = 300$ K and $T_m = 673$ K.

We note that, for a semi-infinitely large solid exposed to low intensities of uniform heat flux, Cohen [5] obtained a similar expression for $X(t)$ using the numerical method of electrical analogy:

$$X(t) = \frac{0.16Q(t - t_m)}{\rho L} \tag{28}$$

where $t_m = \pi k_s^2 \Delta T^2 / 4\kappa_s Q$ is the time to start melting at the surface of a half-space. Eq. (28) significantly underestimates the position of the melting front when compared with the finite element predictions.

4.2. Range of validity

The observed close agreement between the quasi-steady state solutions and the more accurate FEM predictions is perhaps not unexpected, as the melting front in each of the problems considered above moves slowly across the layer, with a velocity $\dot{X}(t)$ typically less than 1 m/s (or, equivalently, $Q < 10^8$ W/m^2). From Eq. (23) it is seen that so long as the applied heat is being completely absorbed by the melting line, i.e., $Q = \rho L \dot{X}$, the method of quasi-steady state should hold (the method is no longer applicable when $X > Q/\rho L$, as shown in the next section). During quasi-steady state melting, the total time t_c needed for a layer of thickness H to completely melt upon heating from the initial temperature T_0 is

$$t_c = t_m + \frac{H\rho L}{Q} \tag{29}$$

where t_m is the time needed to start melting given by Eq. (25). Since the method of quasi-steady state implicitly requires $t_m > t_0$, it follows from Eq. (25) that the applied heat flux must satisfy

$$Q < \frac{2k_s(T_m - T_0)}{H} \tag{30}$$

which requires $Q < 10^8$ W/m^2 for the parameters listed previously for the plotting of Fig. 3. The inequality (30) may be used to gauge whether the quasi-steady state solutions are suitable for a given application. It should also be noticed that these solutions, in general, provide upper limits both for the melt depth and the surface temperature.

On the other hand, given that melting proceeds quasi-steadily under uniform applied heat flux Q, the maximum amount of heat that a phase change layer of thickness H and unit surface area may absorb is

$$\bar{Q} = Qt_c = H\rho L\left\{1 + \frac{c_s(T_m - T_0)}{L}\right\} - 0.3\frac{H^2 Q}{\kappa_s} \tag{31}$$

Obviously, the phase change cooling would lose its usefulness if the duration of the applied heat flux is longer than t_c.

Finally, we note that additional FEM calculations have confirmed that the quasi-steady state solutions are valid for cases where the solid thermal conductivity is different from the melt conductivity; here, the solid and melt conductivities listed in Table 1 are used. The trends are qualitatively similar to that shown in Fig. 3, with the model predictions slightly larger than the FEM results.

5. Solutions for high power densities ($t_m < t_0$)

When the intensity of the applied heat flux exceeds $2k_s(T_m - T_0)/H$, the quasi-steady state solutions are no longer applicable. In this section, two alternative solutions are presented: one based on an approximate analytical technique and the other with the finite element method. The method of finite elements can, in general, account for the latent heat effects, if the mesh is sufficiently refined to allow for temperature gradient discontinuities across the (moving) melting line. The commercial finite element code ABAQUS is used in this paper. As described below, the simple closed-form solutions from the approximate method agree remarkably well with the finite element predictions, particularly so if $t < t_0$.

5.1. Approximate solutions

When the intensity of the applied heat flux is high, it is to be expected that the material starts to melt even before the thermal front reaches the bottom surface of the layer. Mathematically, this may be expressed as

$$\frac{t_m}{t_0} = 4\left[\frac{k_s(T_m - T_0)}{QH}\right] < 1 \tag{32}$$

where $t_0 = H^2/5\kappa_s$ is the thermal penetration time and the first equation of (17) has been used. The above inequality gives the range within which the approximate solutions to be developed below are valid.

Before the thermal front penetrates to the bottom surface $x = H$, the thermal field inside the layer without phase change is the same as that given in Eq. (14) for a half-space thermally insulated at infinity. After the top surface $x = 0$ starts to melt, we assume that the temperature distribution in the molten layer has a profile similar to that without phase changing. In addition, we assume that the thermal properties of the material do not change after melting. Consequently, the fluid temperature is taken as

$$T_l(x, t^*) = T_0 + \frac{Q\sqrt{5\kappa_s(t^* + t_m)}}{2k_s}\left[1 - \frac{x}{\sqrt{5\kappa_s(t^* + t_m)}}\right]^2 \tag{33}$$

where the new time scale t^* starts from the moment melting initiates at the top surface, i.e., $t^* = 0$ when $t = t_m$. Here, the approximate temperature distribution of Eq. (17) is used both for its simplicity as well as accuracy when compared with the exact solution (which is also given in Eq. (17)). Substitution of Eq. (33) into the continuity condition (5) at the melting front leads to

$$X(t^*) = \sqrt{5\kappa_s(t^* + t_m)}\left[1 - \left(\frac{2k_s\Delta T}{Q\sqrt{5\kappa_s(t^* + t_m)}}\right)^{1/2}\right] \tag{34a}$$

where $\Delta T = T_m - T_0$. It follows from Eq. (34a) that the velocity of the melting front is

$$\frac{dX(t^*)}{dt^*} = \sqrt{\frac{5\kappa_s}{4(t^* + t_m)}}\left[1 - \left(\frac{k_s\Delta T}{2Q\sqrt{5\kappa_s(t^* + t_m)}}\right)^{1/2}\right] \tag{34b}$$

Introducing the set of dimensionless parameters $\tilde{X} = X/a$ and $\tilde{t}^* = t^*/(a^2/5\kappa_s)$ with $a = k_s\Delta T/Q$ one can rewrite Eq. (34) as

$$\tilde{X}(\tilde{t}^*) = \sqrt{2}(\tilde{t}^* + 4)^{1/4}\left\{(\tilde{t}^*/4 + 1)^{1/4} - 1\right\} \tag{35a}$$

$$\frac{d\tilde{X}(\tilde{t}^*)}{d\tilde{t}^*} = \frac{(\tilde{t}^* + 4)^{-1/2}}{2}\left\{1 - \frac{(\tilde{t}^* + 4)^{-1/4}}{\sqrt{2}}\right\} \tag{35b}$$

The corresponding evolution of surface temperature with time, expressed in dimensionless form, is

$$\tilde{T}_{surface}(\tilde{t}^*) \equiv \frac{T_{surface}(\tilde{t}^*) - T_0}{T_m - T_0} = (\tilde{t}^*/4 + 1)^{1/2} \tag{36}$$

Observe that the approximate solutions (33), (34) and (36) satisfy the boundary conditions (3) and (5) as well as the initial conditions at the start of melting, namely, $X(t^* = 0) = 0$ and $T_{surface}(t^* = 0) = T_m$, but not the energy balance at the melting front as specified by Eq. (4). The predicted dimensionless melt depth $\tilde{X}$, its velocity $d\tilde{X}/d\tilde{t}^*$, and the temperature rise at the top sur-

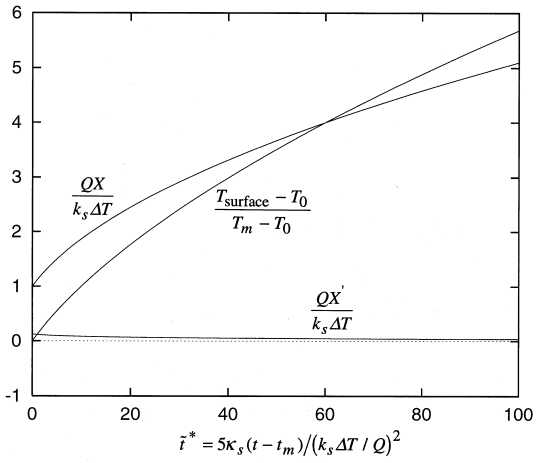

Fig. 4. Dimensionless melt depth $\tilde{X}$, its velocity $d\tilde{X}/d\tilde{t}^*$, and temperature rise at the top surface $(T_{surface}-T_0)/(T_m-T_0)$, as functions of dimensionless time $\tilde{t}^*$ for high intensity levels of applied heat flux ($t_m < t_0$).

face $(T_{surface}-T_0)/(T_m-T_0)$, are plotted in Fig. 4 as functions of dimensionless time $\tilde{t}^*$.

5.2. Finite element solutions

Although simple thermal elements, such as the linear and quadratic elements used in ABAQUS, do not allow discontinuities of temperature gradients (due to latent heat effects) within an element, they do allow such discontinuities between elements. A fine mesh consisting of the lowest order elements, which provide a high number of gradient discontinuity surfaces, is used to simulate the physical problem where the discontinuity of temperature gradients (i.e., the melting front) moves across the mesh. Typically, a total of 2000 elements are used for a layer of thickness $H = 1$ mm. In addition, for high heat flux intensities coupled with large latent heat, the temperature range within which the melting takes place must be carefully specified to avoid numerical instability.

For the same parameters as those used for plotting Fig. 3, Fig. 5 presents the melt depth $X(t)$ and the surface temperature $T_{surface}(t)$ as functions of time for two heat power densities $Q = 10^9$ and $Q = 5\times10^8$ W/m^2. The FEM results plotted as the solid lines agree well with those from the analytical method shown in the dashed lines, if $t < t_0$. Again, this remarkable agreement is somewhat expected, as it can be verified that both cases satisfy the inequality (32), with $t_m/t_0 = 5.565\times10^{-3}$ and $t_m/t_0 = 2.226\times10^{-2}$, respectively. However, the approximate solution (34) for the melt depth $X(t)$ becomes less accurate after the thermal front reaches the bottom surface (namely, when $t > t_0$) wherein the temperature distribution (33) for a half-space thermally insulated at infinity is no longer valid for a finite layer. Thus, for the case $t > t_0$, while the FEM solution predicts an increasing velocity of the melting front as it approaches the bottom surface, the approximate solution (34b) suggests the contrary (Fig. 5(a)). Nevertheless, the evolution of the surface temperature appears to be much less sensitive to the approximate temperature profile (33) even after $t > t_0$, as can be seen from Fig. 5(b).

In contrast to the quasi-steady state solutions for low power densities, the above approximate solutions for high-power densities are only valid for phase change materials having identical solid and melt thermal conductivities. Fortunately, for many materials with solid conductivities smaller than 100 W/(m K), their conductivities do not or only slightly change after

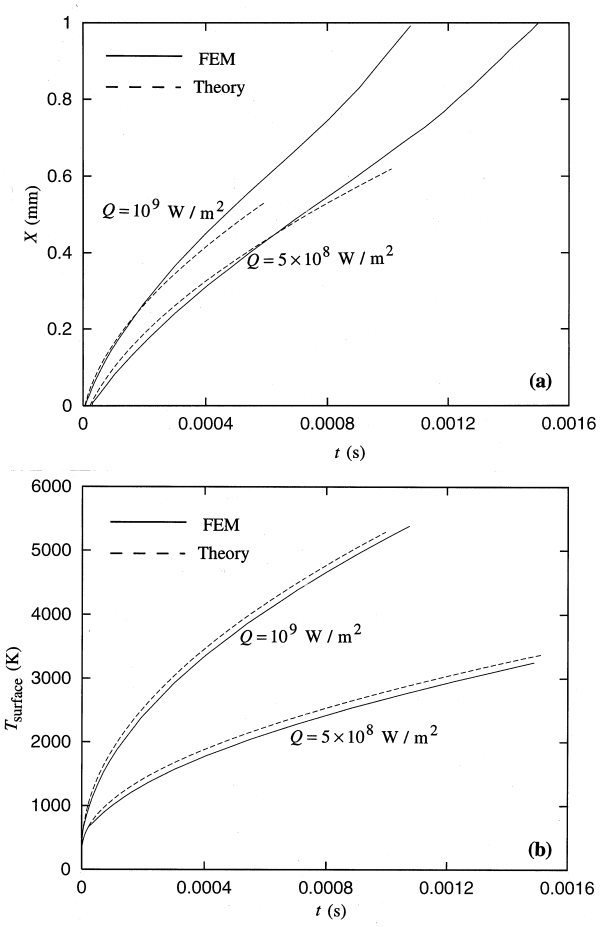

Fig. 5. (a) Melt depth $X(t)$, (b) surface temperature $T_{surface}(t)$ as functions of time for two heat flux intensities: $Q = 10^9$ and $Q = 5\times10^8$ W/m^2. Analytical solutions are represented as dashed lines and FEM results as solid lines. The remaining parameters used are identical to those in Fig. 3.

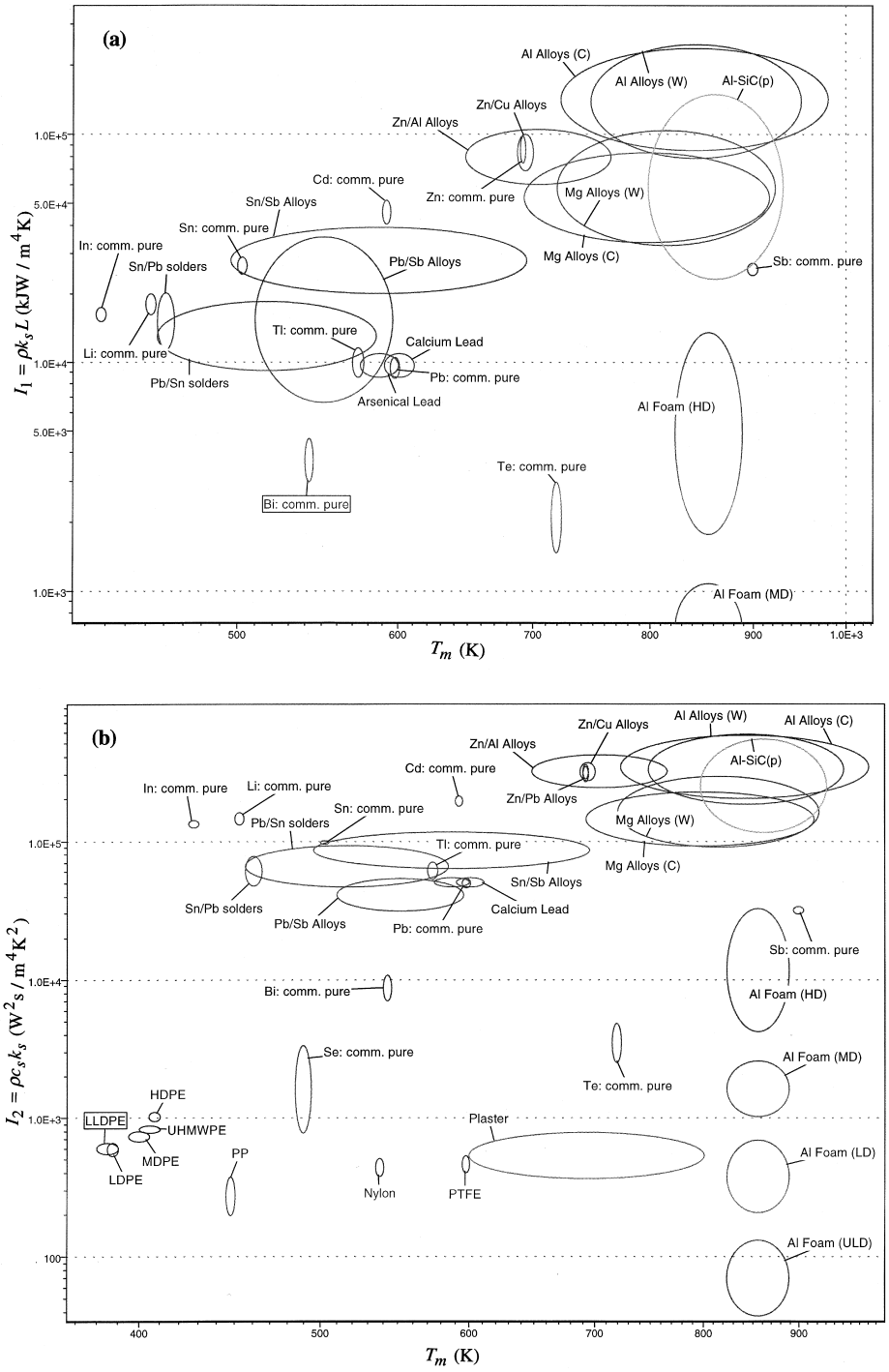

Fig. 6. The materials selection chart of (a) $I_1 = \rho k_s L$, (b) $I_2 = \rho c_s k_s$ versus T_m for phase change cooling.

melting (e.g., titanium and fused quartz, Table 1). For a widely used low temperature phase change material, petroleum wax, its solid conductivity is approximately the same as its melt conductivity ($\sim$0.24 W/(m K)) [19]. For materials with large thermal conductivities ($>$100 W/(m K)), it is not recommended to use the approximate solutions; more accurate method such as finite difference and finite elements should be used.

6. Design implications

During a heat pulse, $Q(\Delta t)$, it is required that the device temperatures remain below an acceptable maximum, T_{max}. Moreover, to take advantage of the phase change, it is also necessary that $T_{max} > T_m$ and that $\Delta t > t_m$. For combination of pulse amplitude and phase change properties such that $t_m < t_0$, Δt is related to the surface temperature by Eq. (34a):

$$\Delta t = \frac{4}{5}\frac{\rho c_s k_s (T_{surface} - T_m)^2}{Q^2} \tag{37}$$

where the condition that T_m should be just above T_0 has been used. Then, the depth of the melting front is obtained from Eq. (34a) as

$$X(\Delta t) = \frac{2k_s(T_{surface} - T_m)}{Q} \tag{38}$$

During the heat pulse, the energy absorbed by the phase change material of initial temperature T_0 is approximately

$$Q\Delta t = \rho L X(\Delta t) + \rho c_s X(\Delta t)(T_m - T_0) \tag{39}$$

Finally, upon substituting Eq. (38) into Eq. (39) and equating $T_{surface}$ to T_{max}, the allowable heat pulse has the form:

$$Q^2\Delta t \le 2\rho k_s L(T_{max} - T_m) + 2\left(k_s^2/\kappa_s\right)(T_{max} - T_m) \times (T_m - T_0) \tag{40}$$

A similar expression can be derived for the case $t_m > t_0$ using quasi-steady state solutions. The result of Eq. (40) suggests that, from a materials selection perspective, the material indices $I_1 = \rho k_s L$ and $I_2 = k_s^2/\kappa_s \equiv \rho c_s k_s$ should be simultaneously maximised. However, under the condition that $T_m \approx T_0$, the first term on the right-hand side of the inequality (40) dominates over the second term, hence the index I_1 plays a more pivotal role in material selection than I_2 does. Fig. 6(a) and (b) present separately the cross-plots of I_1 and I_2 against T_m for all engineering materials, using the Cambridge Materials Selector. For Si, $T_{max} \approx 130$°C and for SiC, $T_{max} \approx 400$°C, suggesting that eutectic alloys containing Sn, Pb, Zn (all having high density ρ and low melting temperature T_m) with limited solid solubilities to obtain high conductivity k_s. Numerical simulations performed for several notional materials (see Table 2) illustrate the role of the phase change in limiting the temperature. The best achievable property combination based on the above calculations, subject to physically realistic limits, is found to be:

$$\rho = 1.5 \times 10^4 \text{ kg/m}^3, \quad c_s = 5000 \text{ J/(kg K)},$$

$$k_s = 150 \text{ W/(m K)}$$

in addition to requiring that $T_m \approx T_0$.

Table 2
Thermophysical properties of several 'notional' eutectic materials

	Sn[c]	Pb[b]	Babbitt alloy[c]
k_s (W/(m K))	45	36	24
κ_s (10^{-6} m^2/s)	24.2	25.3	15.9
ρ (kg/m^3)	8850	10150	10040
T_m (K)	473 ($\pm$16)	503 ($\pm$47)	537 ($\pm$17)
L (10^5 J/kg)	0.41	0.31	1.1

[a] Pb/50Sn solder (ASTM alloy Sn50).
[b] Pb/20Sn solder (ASTM alloy Sn20B).
[c] ASTM Standard B23-83: Alloy 15.

Acknowledgements

The author wishes to thank Prof. M.F. Ashby of Cambridge University, and Profs. A.G. Evans, J.W. Hutchinson and H.A. Stone of Harvard University for insightful discussions on several issues concerning quasi-steady state melting. This work is partially supported by EPSRC, UK and by Rockwell International, USA

Appendix. Effective coefficient of heat transfer

Consider the one-dimensional, steady-state transfer of uniform heat flux Q across a layer of phase change material of thickness H_1 which is bonded to a substrate of thickness H_2, as shown in Fig. A1. Let h_0 denote the heat transfer coefficient at the bottom surface of the substrate $x = H_1 + H_2 \equiv H$, and h the *effective* heat transfer coefficient at the interface $x = H_1$, such that

$$-k_1\frac{\partial T_1}{\partial x} = h(T_1 - T_0), \quad \text{at } x = H_1 \tag{A1}$$

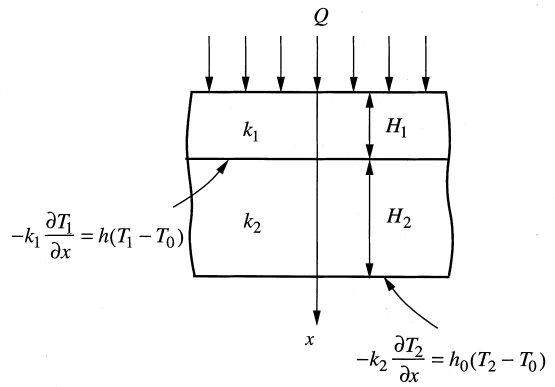

Fig. A1. Geometry and conventions for steady-state heat transfer in a bi-layer system.

$$-k_2\frac{\partial T_2}{\partial x} = h_0(T_2 - T_0), \quad \text{at } x = H \tag{A2}$$

where the subscript '1' is used to denote the thermal constants and temperature of the phase change material, subscript '2' for the corresponding quantities of the substrate, and T_0 is the temperature of the convective medium. In the absence of melting, an elementary analysis of steady-state heat transfer in the bi-layer system results in

$$T_1|_{x=H_1} = T_0 + Q\left(\frac{1}{h_0} + \frac{H_2}{k_2}\right) \tag{A3}$$

$$T_2|_{x=H} = T_0 + \frac{Q}{h_0} \tag{A4}$$

Now, since $-k_1(\partial T_1/\partial x) = -k_2(\partial T_2/\partial x) = Q$ under steady-state, the combination of Eqs. (A1)–(A4) leads to the following expression for the effective heat transfer coefficient h

$$h = \frac{h_0}{1 + Bi} \tag{A5}$$

where $Bi = h_0 H_2/k_2$ is the dimensionless Biot number. For applications considered in this paper, $Bi \ll 1$, hence $h \approx h_0$ is an excellent approximation. For example, $Bi = 10^{-5}$ if $h_0 = 5$ W/(m^2 K) for air convection, $H_2 = 0.5$ mm and $k_2 = 250$ W/(m K) which are representative of the heat sink used in high power electronic packaging.

References

[1] T.J. Lu, A.G. Evans, J.W. Hutchinson, The effects of material properties on heat dissipation in high power electronics, J. Electronic Packaging 120 (1998) 280–289.
[2] T.J. Lu, H.A. Stone, M.A. Ashby, Heat transfer in open-cell metal foams, Acta Mater 46 (1998) 3619–3635.
[3] A.-F. Bastawros, A.G. Evans, H.A. Stone, Evaluation of cellular metal heat dissipation media, J. Heat Transfer (1999), in press.
[4] J.C. Muehlbauer, J.E. Sunderland, Heat conduction with freezing and melting, Applied Mechanics Reviews 18 (1965) 951–957.
[5] M.I. Cohen, Melting of a half-space subjected to a constant heat input, J. Franklin Institute 283 (1967) 271–285.
[6] G. Chen, C.L. Tien, Thermally induced optical nonlinearity during transient heating of thin films, J. Heat Transfer 116 (1994) 311–316.
[7] M.K. El-Adawi, Laser melting of solids: an exact solution for time intervals less or equal to the transit time, J. App. Phys 60 (1986) 2256–2259.
[8] J. Xie, A. Kar, Mathematical modelling of melting during laser materials processing, J. Appl. Phys 81 (1997) 3015–3022.
[9] A. Laouadi, M. Lacroix, Thermal performance of a latent heat energy storage ventilated panel for electric load management, Int. J. Heat Mass Transfer 42 (1999) 275–286.
[10] H.S. Carslaw, J.C. Jaeger, Conduction of Heat in Solids, Oxford University Press, Oxford, 1959.
[11] R.E. Gibson, A heat conduction problem involving a specified moving boundary, Quarterly of Applied Mathematics 16 (1958) 426–430.
[12] B. Rubinsky, A. Shitzer, Analytic solutions to the heat equation involving a moving boundary with applications to the change of phase problem (the inverse Stefan problem), J. Heat Transfer 100 (1978) 300–304.
[13] A. Lazaridis, A numerical solution of the multidimensional solidification (or melting) problem, Int. J. Heat Mass Transfer 13 (1970) 1459–1477.
[14] T.R. Goodman, The heat balance integral and its applications to problems involving change of phase, J. Heat Transfer 80 (1958) 335–341.
[15] M.A. Shannon, B. Rubinsky, R.E. Russo, Detecting laser-induced phase change at the surface of solids via latent heat of melting with a photothermal deflection technique, J. Appl. Phys 75 (1994) 1473–1485.
[16] J.P. Holman, Heat Transfer, McGraw-Hill, New York, 1989.
[17] V.S. Arpaci, Conduction Heat Transfer, Addison-Wesley, Reading, MA, 1966.
[18] T.R. Goodman, J.J. Shea, The melting of finite slabs, J. Appl. Mech 27 (1960) 16–24.
[19] A. Laouadi, M. Lacroix, Thermal performance of a latent heat energy storage ventilated panel for electric load management, Int. J. Heat Mass Transfer 42 (1999) 275–286.